Mueller matrix ellipsometric detection of profile asymmetry in nanoimprinted grating structures

Xiuguo Chen,[1,a)] Chuanwei Zhang,[2,a)] Shiyuan Liu,[1,2,b)] Hao Jiang,[2] Zhichao Ma,[1] and Zhimou Xu[1]
[1]*Wuhan National Laboratory for Optoelectronics, Huazhong University of Science and Technology, Wuhan 430074, China*
[2]*State Key Laboratory of Digital Manufacturing Equipment and Technology, Huazhong University of Science and Technology, Wuhan 430074, China*

(Received 20 August 2014; accepted 7 November 2014; published online 19 November 2014)

Mueller matrix ellipsometry (MME) is applied to detect foot-like asymmetry encountered in nanoimprint lithography (NIL) processes. We present both theoretical and experimental results which show that MME has good sensitivity to both the magnitude and direction of asymmetric profiles. The physics behind the use of MME for asymmetry detection is the breaking of electromagnetic reciprocity theorem for the zeroth-order diffraction of asymmetric gratings. We demonstrate that accurate characterization of asymmetric nanoimprinted gratings can be achieved by performing MME measurements in a conical mounting with the plane of incidence parallel to grating lines and meanwhile incorporating depolarization effects into the optical model. The comparison of MME-extracted asymmetric profile with the measurement by cross-sectional scanning electron microscopy also reveals the strong potential of this technique for in-line monitoring NIL processes, where symmetric structures are desired. © *2014 AIP Publishing LLC*.
[http://dx.doi.org/10.1063/1.4902154]

I. INTRODUCTION

Nanoimprint lithography (NIL),[1,2] in which features on a prepatterned mold are transferred directly into a polymer material, represents a promising technique with the potential for high resolution and throughput as well as low cost. Although symmetric imprint resist profiles are expected in most cases, errors could occur in actual NIL processes and will result in undesired asymmetry and pattern transfer fidelity loss in downstream processes. Detection of imprint resist asymmetric defects leads to improvement of the template, imprint process, and imprint tooling design, and therefore guarantees pattern transfer fidelity in template replication. Both cross-sectional scanning electron microscopy (X-SEM) and atomic force microscopy (AFM) are capable of identifying imprint resist profile asymmetry, but they are in general time-consuming, expensive, complex to operate, and problematic in realizing in-line integrated measurements. Being nondestructive, inexpensive and time-effective, optical scatterometry, which is traditionally based on reflectometry and ellipsometry, has been successfully introduced to characterize nanoimprinted grating structures.[3–5] However, conventional optical scatterometry techniques have difficulties in measuring asymmetric grating structures due to the lack of capability of distinguishing the direction of profile asymmetry.[6,7]

In this work, we apply Mueller matrix ellipsometry (MME, sometimes also referred to as Mueller matrix polarimetry) to characterize nanoimprinted grating structures with foot-like asymmetric profiles that were encountered in our NIL processes when the processes were not operated at optimum conditions. Compared with conventional optical scatterometry, which at most obtains two ellipsometric angles Ψ and Δ, MME-based scatterometry can provide up to 16 quantities of a 4×4 Mueller matrix in each measurement and can thereby acquire much more useful information about the sample. In our recent work, MME was applied to characterize nanoimprinted grating structures with symmetric profiles.[8,9] We experimentally demonstrated that improved accuracy can be achieved for the line width, line height, sidewall angle, and residual layer thickness characterization by performing MME measurements in the optimal measurement configuration and meanwhile using the additional depolarization information contained in the measured Mueller matrices. The present work will further show that MME not only has good sensitivity to both the magnitude and direction of profile asymmetry, but also can be applied to accurately characterize asymmetric nanoimprinted gratings by fully exploiting the rich information hidden in the measured Mueller matrices.

II. EXPERIMENT

Figure 1 depicts the X-SEM image of the investigated nanoimprinted grating structure, which was obtained from a ~240 nm STU220 resist film (developed by Obducat AB Co.) on a Si wafer substrate imprinted on an Eitre3 Nano Imprinter using a Si imprinting mold. The Si mold fabricated by e-beam lithography followed by dry etching has gratings with a period of 800 nm, a top line width of 350 nm, a line height of 472 nm, and a sidewall angle of 88°.[10] It can be easily observed that the nanoimprinted grating structure depicted in Fig. 1 does not have a symmetric profile, but

[a)]X. Chen and C. Zhang contributed equally to this work.
[b)]Author to whom correspondence should be addressed. Electronic mail: shyliu@mail.hust.edu.cn

shows a foot-like asymmetry. As shown in Fig. 1, the foot-like asymmetric profile can be roughly divided into two segments, and each segment seems unable to be characterized with a simple trapezoidal geometric model as did in our previous work.[8,9] We thereby adopted a two-segment quadratic geometric model to characterize the foot-like asymmetry (the traditional trapezoidal model can be viewed as a linear geometric model). For each segment i, the total height is H_i, the width and profile offset at a given point z measured down from the top of the segment are given by

$$w_i(z) = \{a_{i0} + a_{i1}[(z - H_{i-1})/H_i] + a_{i2}[(z - H_{i-1})/H_i]^2\}\Lambda, \tag{1a}$$

$$\delta_i(z) = \{b_{i0} + b_{i1}[(z - H_{i-1})/H_i] + b_{i2}[(z - H_{i-1})/H_i]^2\}\Lambda, \tag{1b}$$

respectively. Here, a_{ij} and b_{ij} ($i = 1, 2$; $j = 0, 1, 2$) are undetermined coefficients, Λ is the grating pitch, which is expected to be equal to the period of the Si mold. H_0 is specified to be 0 to make Eq. (1) valid when $i = 1$. b_{10} is set to be 0 since there is no offset at the top of the 1st segment. In addition, Eq. (1) should satisfy the boundary conditions, i.e., $w_1(H_1) = w_2(H_1)$ and $\delta_1(H_1) = \delta_2(H_1)$ due to the continuity of the grating line profile. According to the boundary conditions, we obtain that $a_{20} = a_{10} + a_{11} + a_{12}$ and $b_{20} = b_{11} + b_{12}$. Hence, there are totally 11 undetermined parameters if we assume $\Lambda = 800$ nm. It is noted that the geometric model given in Eq. (1) can be readily extended to high-order shapes with much more undetermined parameters. However, further parameterization would result in asymmetric profiles with poor confidence limits and would even yield physically meaningless or incorrect results.

We used an in-house developed dual rotating-compensator Mueller matrix ellipsometer[9,11] to collect the Mueller matrix ellipsometric data of the investigated nanoimprinted grating structure. With this dual rotating-compensator layout, the full Mueller matrix elements can be obtained in a single measurement. The spectral range of the ellipsometer is from 200 to 1000 nm. The beam diameter can be changed from the normal value of ~3 mm to a value less than 200 μm with the focusing lens. The two arms of the instrument and the sample stage can be rotated to choose the incidence angle θ and azimuthal angle ϕ (angle between the plane of incidence and the direction of grating pitch) for maximum sensitivity to the foot-like asymmetry. In the data analysis, the optical constants of the Si substrate were fixed at values taken from the literature.[12] The optical properties of the STU220 resist film were modeled using a two-term Forouhi-Bloomer model,[13] whose parameters were determined from a STU220 resist film deposited on the Si substrate and taken as $A_1 = 4.447\text{e}-3$, $A_2 = 3.051\text{e}-2$, $B_1 = 8.8611$ eV, $B_2 = 12.0043$ eV, $C_1 = 19.6703$ eV^2, $C_2 = 36.3258$ eV^2, $n(\infty) = 1.4842$, and $E_g = 3.3724$ eV.

III. THEORY

Theoretical Mueller matrices of a grating sample can be calculated by rigorous coupled-wave analysis (RCWA).[14–16] In RCWA, both the permittivity function and electromagnetic fields are expanded into Fourier series. Afterwards, the tangential filed components are matched at boundaries between different layers, and thereby the boundary-value problem is reduced to an algebraic eigenvalue problem. Consequently, the overall reflection coefficients can be calculated by solving this eigenvalue problem. According to the reflection coefficients, the 2×2 Jones matrix $\mathbf{J}$ associated with the zeroth-order diffracted light of the sample, which connects the incoming Jones vector with the diffracted one, can be formulated by

$$\begin{bmatrix} E_{rp} \\ E_{rs} \end{bmatrix} = \mathbf{J} \begin{bmatrix} E_{ip} \\ E_{is} \end{bmatrix} = \begin{bmatrix} r_{pp} & r_{ps} \\ r_{sp} & r_{ss} \end{bmatrix} \begin{bmatrix} E_{ip} \\ E_{is} \end{bmatrix}, \tag{2}$$

where $E_{s,p}$ refers to the electric field component perpendicular and parallel to the plane of incidence, respectively. In the absence of depolarization, the 4×4 Mueller matrix $\mathbf{M}$ can be calculated from the Jones matrix $\mathbf{J}$ by[17]

$$\mathbf{M} = \begin{bmatrix} \frac{1}{2}\left(|r_{pp}|^2 + |r_{sp}|^2 + |r_{ps}|^2 + |r_{ss}|^2\right) & \frac{1}{2}\left(|r_{pp}|^2 + |r_{sp}|^2 - |r_{ps}|^2 - |r_{ss}|^2\right) & \mathrm{Re}\left(r_{pp}r_{ps}^* + r_{sp}r_{ss}^*\right) & \mathrm{Im}\left(r_{pp}r_{ps}^* + r_{sp}r_{ss}^*\right) \\ \frac{1}{2}\left(|r_{pp}|^2 - |r_{sp}|^2 + |r_{ps}|^2 - |r_{ss}|^2\right) & \frac{1}{2}\left(|r_{pp}|^2 - |r_{sp}|^2 - |r_{ps}|^2 + |r_{ss}|^2\right) & \mathrm{Re}\left(r_{pp}r_{ps}^* - r_{sp}r_{ss}^*\right) & \mathrm{Im}\left(r_{pp}r_{ps}^* - r_{sp}r_{ss}^*\right) \\ \mathrm{Re}\left(r_{pp}r_{sp}^* + r_{ps}r_{ss}^*\right) & \mathrm{Re}\left(r_{pp}r_{sp}^* - r_{ps}r_{ss}^*\right) & \mathrm{Re}\left(r_{pp}r_{ss}^* + r_{ps}r_{sp}^*\right) & \mathrm{Im}\left(r_{pp}r_{ss}^* - r_{ps}r_{sp}^*\right) \\ -\mathrm{Im}\left(r_{pp}r_{sp}^* + r_{ps}r_{ss}^*\right) & -\mathrm{Im}\left(r_{pp}r_{sp}^* - r_{ps}r_{ss}^*\right) & -\mathrm{Im}\left(r_{pp}r_{ss}^* + r_{ps}r_{sp}^*\right) & \mathrm{Re}\left(r_{pp}r_{ss}^* - r_{ps}r_{sp}^*\right) \end{bmatrix}, \tag{3}$$

where Re(·) and Im(·) represent the real and imaginary parts of a complex number, respectively. Specifically, when the plane of incidence is perpendicular to grating lines, i.e., with the azimuthal angle $\phi = 0°$, cross-polarization reflection coefficients r_{ps} and r_{sp} are zero for any periodic structure. In this case, the Mueller matrix $\mathbf{M}$ can be expressed in terms of conventional ellipsometric angles Ψ and Δ (which are generally used to characterize isotropic samples) and is expressed as follows:

$$\mathbf{M} = \frac{1}{2}\left(|r_{pp}|^2 + |r_{ss}|^2\right)\begin{bmatrix} 1 & -\cos 2\Psi & 0 & 0 \\ -\cos 2\Psi & 1 & 0 & 0 \\ 0 & 0 & \sin 2\Psi \cos\Delta & \sin 2\Psi \sin\Delta \\ 0 & 0 & -\sin 2\Psi \sin\Delta & \sin 2\Psi \cos\Delta \end{bmatrix}. \quad (4)$$

The normalizing multiplication factor in Eq. (4) is also referred to as sample reflectivity.

In practice, the measurement process invariably has depolarization effects due to the factors existing in the measurement system and the measured sample *per se*, such as finite spectral bandwidth of the monochromator, finite numerical aperture (NA) of the focusing lens, thickness nonuniformity in a thin film formed on a substrate, and large surface or edge roughness of a sample.[8,9] The depolarization phenomena caused by the above factors essentially occur by the generation of different polarizations upon light reflection and are generally referred to as quasi-depolarization. In the presence of depolarization, totally polarized light used as a probe in ellipsometry is transformed into partially polarized light, and the Jones matrix formalism cannot be used to describe the optical response of this sample any more, while the Mueller matrix formalism is still applicable. In this case, the associated Mueller matrix is a depolarizing one. The depolarization effect of a depolarizing Mueller matrix $\mathbf{M}$ can be characterized by the depolarization index DI defined by[18]

$$DI = \left[\frac{\mathrm{Tr}(\mathbf{M}\mathbf{M}^{\mathrm{T}}) - m_{11}^2}{3m_{11}^2}\right]^{1/2}, \quad 0 \le DI \le 1, \quad (5)$$

where $\mathbf{M}^{\mathrm{T}}$ is the transpose of $\mathbf{M}$ and $\mathrm{Tr}(\cdot)$ represents the matrix trace. $DI = 0$ and $DI = 1$ correspond to the totally depolarizing and non-depolarizing Mueller matrices, respectively. In the analysis of a depolarizing sample, Eq. (3) cannot be applied to directly derive the Mueller matrix from the corresponding Jones matrix. The optical modeling principle is based on the optical equivalence of the polarization states,[19] which states that a depolarizing system is optically equivalent to a system composed of a parallel combination of several non-depolarizing systems. We further deduce that a depolarizing Mueller matrix can be written as the sum of various non-depolarizing Mueller matrices, i.e.[9]

$$\mathbf{M}^{\mathrm{D}} = \int \rho(\mathbf{x})\mathbf{M}^{\mathrm{ND}}(\mathbf{x})d\mathbf{x}, \quad (6)$$

where $\mathbf{M}^{\mathrm{D}}$ and $\mathbf{M}^{\mathrm{ND}}$ represent the depolarizing and non-depolarizing Mueller matrices, respectively, and the latter can be calculated by Eq. (3). The variable $\mathbf{x}$ denotes the factors that induce depolarization, and $\rho(\mathbf{x})$ is a weighting function, which can be specifically the spectral bandwidth function, NA, or thickness distribution function, etc.

A weighted least-squares regression analysis (Levenberg-Marquardt algorithm[20]) is then performed, during which the measurands are varied until the calculated and measured data match as close as possible. This is done by minimizing a weighted mean square error function χ_r^2 defined by

$$\chi_r^2 = \frac{1}{15N - P}\sum_{k=1}^{N}\sum_{i,j=1}^{4}\left[\frac{m_{ij,k}^{\mathrm{meas}} - m_{ij,k}^{\mathrm{calc}}}{\sigma(m_{ij,k})}\right]^2, \quad (7)$$

where k indicates the k-th spectral point from the total number N, indices i and j show all the Mueller matrix elements except m_{11} (normalized to m_{11}), P is the total number of measurands, $m_{ij,k}^{\mathrm{meas}}$ and $m_{ij,k}^{\mathrm{calc}}$ denote the measured and calculated Mueller matrix elements, respectively, and $\sigma(m_{ij,k})$ is the estimated standard deviation associated with $m_{ij,k}$.

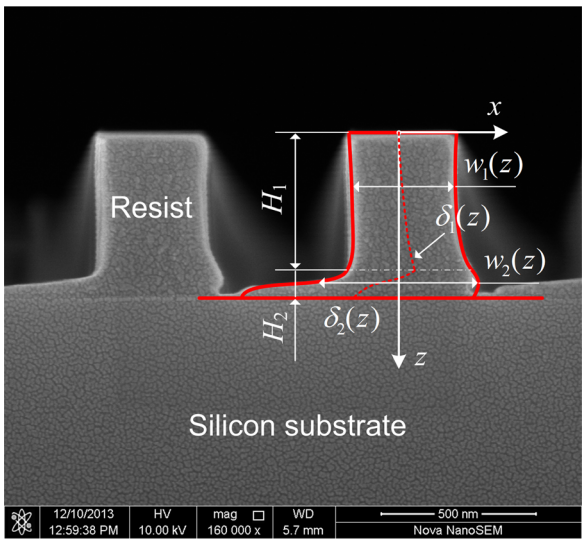

FIG. 1. X-SEM micrograph and geometric model of the investigated nanoimprinted grating structure.

IV. RESULTS AND DISCUSSION

To examine the sensitivity of MME to the direction and magnitude of profile asymmetry, we have simulated the Mueller matrix spectra for a grating test structure with asymmetric profiles in different azimuthal angles. The grating structure is similar to that shown in Fig. 1 but is characterized with a one-segment quadratic grating line shape and a uniform residual resist layer. The quadratic grating line shape has a period of 800 nm, a line height of 475 nm, and takes $a_0 = 0.44$, $a_1 = -0.040$, $a_2 = 0.12$ for the line width, $b_1 = -0.010$, $b_2 = 0.035$ for a positive (right) profile offset ($\delta > 0$), and $b_1 = 0.010$, $b_2 = -0.035$ for a negative (left) profile offset ($\delta < 0$). The residual resist thickness is 45 nm. Figure 2 depicts the difference Mueller matrix spectra

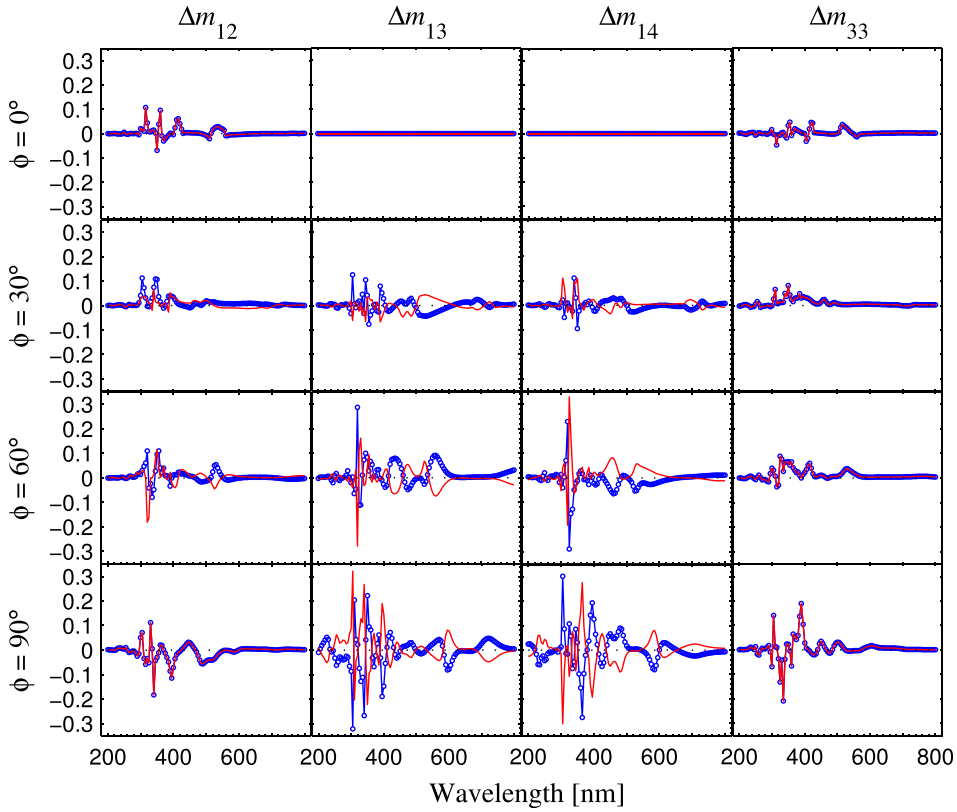

FIG. 2. The difference spectra of Mueller matrix elements m_{12}, m_{13}, m_{14}, and m_{33} between that calculated for the grating test structure with asymmetric and symmetric profiles in different azimuthal angles. The red solid curves and the blue solid curves with open circles correspond to asymmetric profiles with positive (right) and negative (left) offsets, respectively.

between that calculated for the grating test structure with asymmetric ($b_1 = \mp 0.010$, $b_2 = \pm 0.035$) and symmetric ($b_1 = 0$, $b_2 = 0$) profiles using RCWA. The incidence angle θ is fixed at 65°, and the azimuthal angle ϕ is varied from 0° to 90° with increments of 30°. We chose 4 typical elements m_{12}, m_{13}, m_{14}, and m_{33} from the 4×4 normalized Mueller matrix, of which m_{12} and m_{33} are, respectively, equal to $\alpha = -\cos 2\Psi$ and $\beta = \sin 2\Psi \cos \Delta$ in conventional ellipsometric scatterometry[5,21] when $\phi = 0°$ and m_{13} and m_{14} are elements from the upper right 2×2 off-diagonal block of the Mueller matrix. In addition, m_{12}, m_{13}, and m_{14} are also the elements of the diattenuation vector of the normalized Mueller matrix, which correspond to the horizontal, 45°-linear and circular diattenuations, respectively.[22] As shown in Fig. 2, when $\phi = 0°$, m_{12} and m_{33} are only sensitive to the magnitude of profile asymmetry, which indicates that conventional ellipsometric scatterometry is indeed incapable of distinguishing the positive and negative profile offsets. When $\phi = 0°$, m_{13} and m_{14} are insensitive to the magnitude and direction of profile asymmetry. However, when $\phi \neq 0°$, m_{13} and m_{14} exhibits noticeable sensitivity to both the magnitude and direction of profile asymmetry especially when $\phi = 90°$ and in this case $\Delta m_{13}(\delta > 0) = -\Delta m_{13}(\delta < 0)$ and $\Delta m_{14}(\delta > 0) = -\Delta m_{14}(\delta < 0)$. It can be also observed from Fig. 2 that m_{12} also shows slight disparity in its difference spectra for asymmetric profiles with positive and negative offsets when $\phi = 30°$ and $\phi = 60°$, while m_{33} always exhibits insensitivity to the direction of profile asymmetry even when $\phi \neq 0°$.

An intuitive interpretation of the results shown in Fig. 2 is that when $\phi = 0°$, i.e., with the plane of incidence perpendicular to grating lines, all the light is incident upon one side of the asymmetric profile, while the other side does not receive any light. Therefore, the shadowing effect will attenuate the sensitivity to the direction of profile asymmetry. However, when the plane of incidence is not perpendicular to grating lines, i.e., $\phi \neq 0°$, since both sides of the asymmetric profile can receive light, the corresponding Mueller matrix spectra, thus, exhibit improved sensitivity to the direction of profile asymmetry. Moreover, since the two sides of the asymmetric profile do not receive the same amount of irradiance when $\phi = 30°$ and $\phi = 60°$, the absolute difference Mueller matrix spectra corresponding to the positive and negative offsets will not be equal, as indicated in Fig. 2. In contrast, when $\phi = 90°$, i.e., with the plane of incidence parallel to grating lines, the two sides of the asymmetric profile receive the same amount of irradiance, therefore the absolute difference Mueller matrix spectra corresponding to the positive and negative offsets are equal. From this aspect, it is expected that the Mueller matrix spectra at $\phi = 90°$ will be most sensitive to profile asymmetry. The root-mean-square error between the Mueller matrix spectra for the grating structure with asymmetric and symmetric profiles were calculated at different azimuthal angles. As expected, the Mueller matrix spectra at $\phi = 90°$ indeed demonstrate the greatest sensitivity.

The physics behind the use of MME for profile asymmetry detection is the electromagnetic reciprocity theorem for the zeroth-order diffraction of symmetric gratings,[23] which states that, for any incident light (θ, ϕ), the zeroth-order cross-polarization reflection coefficients r_{ps} and r_{sp} of a grating sample are antisymmetric, i.e., $r_{ps} = -r_{sp}$, provided that the grating is composed of only reciprocal materials and is invariant under the rotation of 180° about the normal

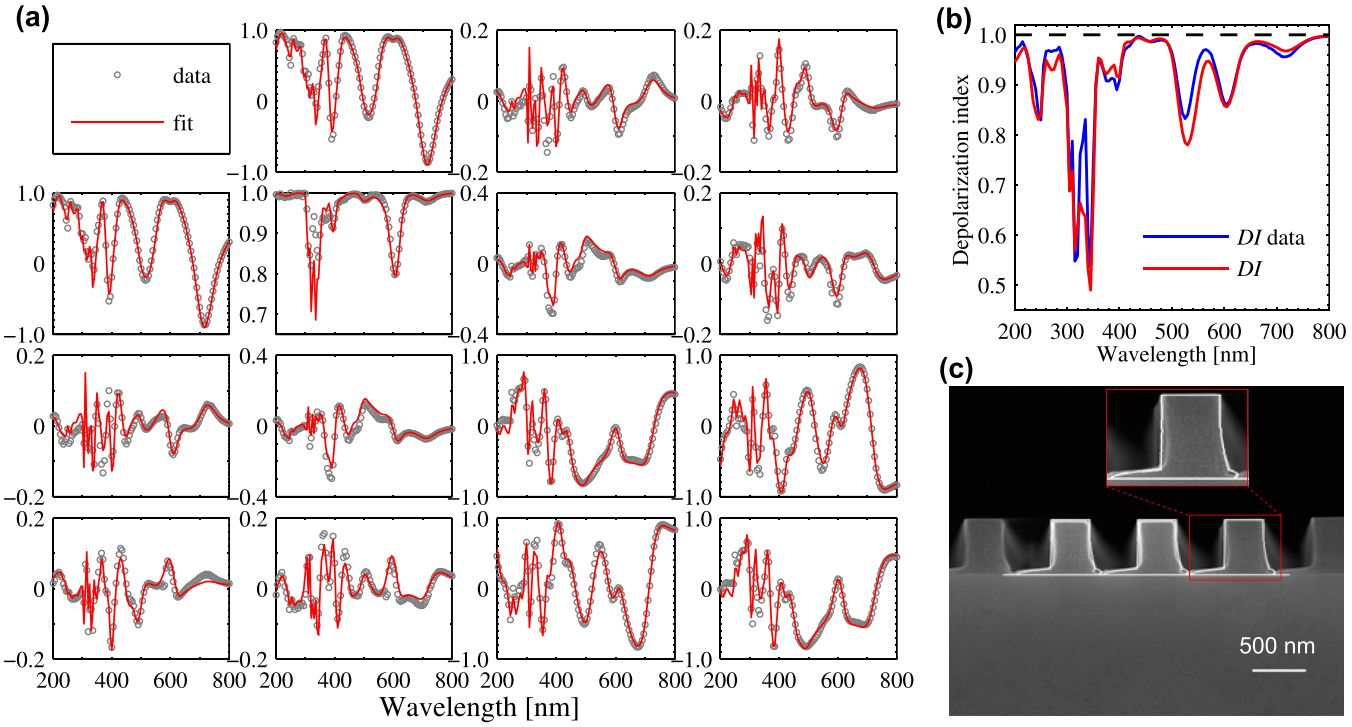

FIG. 3. (a) Fitting result and (b) depolarization index spectra of the measured and calculated best-fit Mueller matrix spectra when considering the depolarization effects induced by finite spectral bandwidth and NA. (c) X-SEM micrograph of the investigated nanoimprinted grating structure shown in Fig. 1 with the reconstructed two-segment quadratic line shape overlaid.

incidence. According to this reciprocity theorem and Eq. (3), we can further derive the relations between the elements of the two 2×2 off-diagonal blocks of the Mueller matrix that $m_{13}+m_{31}=0$, $m_{23}+m_{32}=0$, $m_{14}-m_{41}=0$, and $m_{24}-m_{42}=0$. When the profile is asymmetric, the above reciprocity is broken and we have $r_{ps}\neq -r_{sp}$ and $|m_{ij}|\neq|m_{ji}|$ $(i=1,\,2;\,j=3,\,4)$. Among the various azimuthal configurations, two special cases are of great interest. The first case is that when $\phi=0^\circ$ all diffracted orders of reflected beams are within the plane of incidence and this configuration is usually called planar diffraction. In this case, the relation $r_{ps}=-r_{sp}$ is trivially satisfied because both r_{ps} and r_{sp} are zero for any periodic structure even if it has an asymmetric profile. Then, the two 2×2 off-diagonal blocks of the Mueller matrix vanish, as described in Eq. (4). Therefore, m_{13} does not show any sensitivity to profile asymmetry, as depicted in Fig. 2. Another case is that when $\phi=90^\circ$ all diffracted orders of reflected beams are on the surface of a cone with revolution symmetry about the direction of grating lines and this configuration is usually called conical diffraction. In this case, the relation $r_{ps}=-r_{sp}$ is also trivially satisfied because both r_{ps} and r_{sp} are zero for symmetric gratings. However, for asymmetric gratings, both r_{ps} and r_{sp} as well as the two 2×2 off-diagonal blocks of the Mueller matrix will be different from zero. Moreover, for profile offsets with the same magnitude and opposite direction, the elements of the 2×2 off-diagonal blocks of the Mueller matrix will exhibit the same absolute deviation from zero with opposite sign, as illustrated in Fig. 2. It is worth pointing out that the above properties of Mueller matrices can still be applicable even in the presence of depolarization effects that maybe induced by instrumental finite spectral bandwidth and NA, etc.

We have also conducted an experimental demonstration of detection of the foot-like asymmetry shown in Fig. 1. The measured Mueller matrix spectra that were collected in the specular mode at the incidence angle of 65° and azimuthal angle of 90° are presented in Fig. 3(a). It is observed from Fig. 3(a) that the two 2×2 off-diagonal blocks of the Mueller matrix spectra are not equal to zero, which therefore again demonstrates the sensitivity to the foot-like asymmetry. In addition, Fig. 3(b) presents the depolarization index spectrum calculated using Eq. (5) that corresponds to the measured Mueller matrix spectra shown in Fig. 3(a). As can be observed from Fig. 3(b), the depolarization indices exhibit great deviation from 1 over most of the spectrum and show significant dips to ~0.55 near 310 nm and 340 nm. Clearly, the depolarization effects shown in Fig. 3(b) should not be

TABLE I. Extracted parameter values for the fits shown in Fig. 3(a).

Parameter	Value	95% conf. limit	Unit
a_{10}	0.457	0.0018	Intercept
a_{11}	−0.057	0.0090	Slope
a_{12}	0.127	0.0106	Curvature
b_{11}	−0.014	0.0038	Slope
b_{12}	0.042	0.0041	Curvature
a_{21}	1.077	0.1402	Slope
a_{22}	−0.663	0.2070	Curvature
b_{21}	−0.288	0.0617	Slope
b_{22}	0.108	0.0967	Curvature
H_1	459.643	2.0638	Nm
H_2	62.136	2.0831	Nm

TABLE II. Correlation coefficients for the parameters in Table I.

	a_{10}	a_{11}	a_{12}	b_{11}	b_{12}	a_{21}	a_{22}	b_{21}	b_{22}	H_1	H_2
a_{10}	1										
a_{11}	−0.884	1									
a_{12}	0.663	−0.928	1								
b_{11}	−0.065	0.039	−0.025	1							
b_{12}	0.064	−0.021	−0.006	−0.972	1						
a_{21}	0.155	−0.260	0.307	−0.278	0.275	1					
a_{22}	−0.126	0.239	−0.289	0.284	−0.278	−0.987	1				
b_{21}	0.041	−0.241	0.399	0.040	−0.120	0.639	−0.621	1			
b_{22}	−0.011	0.203	−0.341	0.065	0.002	−0.776	0.799	−0.927	1		
H_1	0.190	−0.398	0.538	−0.174	0.129	0.839	−0.800	0.743	−0.755	1	
H_2	−0.251	0.468	−0.612	0.176	−0.132	−0.818	0.778	−0.738	0.741	−0.992	1

ignored but be included in the interpretation of the measured data.

In our recent work, we have demonstrated that the depolarization effects observed from measured data of nanoimprinted gratings are mainly induced by the finite spectral bandwidth and NA of the ellipsometer, as well as thickness variation of the residual resist layer.[8,9] However, as shown in Fig. 1, the always existent residual resist layer at the bottom of the imprinted features is discontinuous near the "heel" of the foot-like asymmetry, which makes it also like imprinted features. There does not exist an observable residual resist film layer between the imprinted features and the Si substrate in Fig. 1. We thereby only consider the depolarization effects induced by the finite spectral bandwidth and NA in the interpretation of the measured data. The instrumental spectral bandwidth and NA were pre-determined through a measurement on a nominally 1000 nm SiO_2 thick thermal film on the Si substrate to isolate the effects of finite bandwidth and NA from sample-specific artifacts. The measurement yielded a spectral bandwidth of 1.0 nm and a NA of 0.065. In addition, before incorporating the depolarization effects into the interpretation of the measured data, we also compared the fitting results achieved by fixing and by varying the azimuthal angle, respectively. The comparison revealed that there was a slight misalignment of about 0.07° in the azimuthal angle and this misalignment had a negligible impact on the final fitting results. To decrease the RCWA calculation time, we fixed the bandwidth, NA and azimuthal angle and let just the model parameters a_{10}, a_{11}, a_{12}, b_{11}, b_{12}, a_{21}, a_{22}, b_{21}, b_{22}, H_1, and H_2 vary in the regression analysis (grating pitch was fixed at the nominal value of 800 nm).

Figure 3(a) shows the fitting result of the measured and calculated best-fit Mueller matrix spectra when taking the depolarization effects induced by finite spectral bandwidth and NA into account. Figure 3(b) depicts the depolarization index spectra for the measured and calculated best-fit Mueller matrix spectra shown in Fig. 3(a). As can be observed from Figs. 3(a) to 3(b), the measured and calculated Mueller matrix spectra as well as the associated depolarization index spectra show a good agreement over most of the spectrum. Small differences in the fitting result and depolarization index spectra near 330 nm can also be observed from Figs. 3(a) to 3(b), which indicates that there may be still some room for improvement in the adopted geometric model on the one hand and on the other hand there may be some unknown sources of depolarization that we did not take into account. Anyway, the results shown in Figs. 3(a) and 3(b) have demonstrated the capability of MME for the detection of asymmetry in nanoimprinted gratings. The extracted parameter values and the associated uncertainties with a 95% confidence level for the fit shown in Fig. 3(a) are presented in Table I. The uncertainty in the ith parameter was estimated by $1.96 \times \chi_r \times \sqrt{C_{ii}}$, where C_{ii} is the ith diagonal element of the fitting parameter covariance matrix.[24] Figure 3(c) depicts the X-SEM micrograph of the investigated nanoimprinted grating structure shown in Fig. 1 overlapped with the two-segment quadratic line shape reconstructed using the parameters given in Table I. As shown in Fig. 3(c), the reconstructed asymmetric profile exhibits a good match with the X-SEM image apart from a slight difference in the "heel" of the foot-like asymmetry. Table II presents the correlation coefficients for the parameters in Table I. From Table II, the slope and curvature terms of the width and profile offset models given in Eq. (1) as well as the total heights of the two segments show relatively strong coupling, which indicates the difficulty in clearly resolving these parameters. It is worth pointing out that the parameter correlation would be further decreased by performing regression analysis for a single azimuthal angle, with multiple incidence angles together, which has been reported in Ref. 25. As this is a rather time consuming procedure, especially when further taking the depolarization effects into account, we did not perform this analysis in this work. Anyway, considering that all of the fitting parameters exhibit confidence limits that are less than the parameters themselves shown in Table I, we have pushed the data to the limit of statistical merit.

V. CONCLUSIONS

In this work, nanoimprinted grating structures with foot-like asymmetric profiles that were encountered in our NIL processes were characterized using an in-house developed Mueller matrix ellipsometer. We have demonstrated that MME has good sensitivity to both the magnitude and direction of the foot-like asymmetry especially in a conical

mounting with the plane of incidence parallel to grating lines. Accurate characterization of asymmetric nanoimprinted gratings has been achieved by performing MME measurements in this conical mounting and incorporating the depolarization effects induced by the finite spectral bandwidth and NA of the ellipsometer into the interpretation of the measured data. It is worth mentioning that the presented technique is not limited to detection of the reported foot-like asymmetry. It generally can be extended to characterize other kinds of asymmetric profiles encountered in practical NIL processes.

ACKNOWLEDGMENTS

This work was funded by the National Natural Science Foundation of China (Grant Nos. 51475191 and 51405172), the National Instrument Development Specific Project of China (Grant No. 2011YQ160002), and the Program for Changjiang Scholars and Innovative Research Team in University of China. The authors would like to thank the facility support of the Center for Nanoscale Characterization and Devices, Wuhan National Laboratory for Optoelectronics (WLNO) (Wuhan, China).

[1]S. Y. Chou, P. R. Krauss, and P. J. Renstrom, Science **272**, 85 (1996).
[2]S. Y. Chou, P. R. Krauss, W. Zhang, L. Guo, and L. Zhuang, J. Vac. Sci. Technol. B **15**, 2897 (1997).
[3]D. Fuard, C. Perret, V. Farys, C. Gourgon, and P. Schiavone, J. Vac. Sci. Technol. B **23**, 3069 (2005).
[4]R. M. Al-Assaad, S. Regonda, L. Tao, S. W. Pang, and W. Hu, J. Vac. Sci. Technol. B **25**, 2396 (2007).
[5]H. J. Patrick, T. A. Germer, Y. Ding, H. W. Ro, L. J. Richter, and C. L. Soles, Appl. Phys. Lett. **93**, 233105 (2008).
[6]T. Novikova, A. De Martino, R. Ossikovski, and B. Drévillon, Eur. Phys. J.: Appl. Phys. **31**, 63 (2005).
[7]J. Li, J. J. Hwu, Y. Liu, S. Rabello, Z. Liu, and J. Hu, J. Micro/Nanolithogr. MEMS MOEMS **9**, 041305 (2010).
[8]X. G. Chen, C. W. Zhang, and S. Y. Liu, Appl. Phys. Lett. **103**, 151605 (2013).
[9]X. G. Chen, S. Y. Liu, C. W. Zhang, H. Jiang, Z. C. Ma, T. Y. Sun, and Z. M. Xu, Opt. Express **22**, 15165 (2014).
[10]X. G. Chen, S. Y. Liu, C. W. Zhang, and H. Jiang, J. Micro/Nanolithogr. MEMS MOEMS **12**, 033013 (2013).
[11]S. Y. Liu, X. G. Chen, and C. W. Zhang, ECS Trans. **60**, 237 (2014).
[12]C. H. Herzinger, B. Johs, W. A. McGahan, J. W. Woollam, and W. Paulson, J. Appl. Phys. **83**, 3323 (1998).
[13]A. R. Forouhi and I. Bloomer, Phys. Rev. B **38**, 1865 (1988).
[14]M. G. Moharam, E. B. Grann, D. A. Pommet, and T. K. Gaylord, J. Opt. Soc. Am. A **12**, 1068 (1995).
[15]L. Li, J. Opt. Soc. Am. A **13**, 1870 (1996).
[16]S. Y. Liu, Y. Ma, X. G. Chen, and C. W. Zhang, Opt. Eng. **51**, 081504 (2012).
[17]R. M. A. Azzam and N. M. Bashara, *Ellipsometry and Polarized Light* (North-Holland, Netherland, 1977).
[18]J. J. Gil and E. Bernabeu, Opt. Acta **33**, 185 (1986).
[19]H. C. van de Hulst, *Light Scattering by Small Particles* (Wiley, New York, 1957).
[20]W. H. Press, S. A. Teukolsky, W. T. Vetterling, and B. P. Flannery, *Numerical Recipes: The Art of Scientific Computing*, 3rd ed. (Cambridge University Press, Cambridge, 2007).
[21]H. T. Huang and F. L. Terry, Jr., Thin Solid Films **468**, 339 (2004).
[22]S. Y. Lu and R. A. Chipman, J. Opt. Soc. Am. A **13**, 1106 (1996).
[23]L. Li, J. Opt. Soc. Am. A **17**, 881 (2000).
[24]X. G. Chen, S. Y. Liu, H. G. Gu, and C. W. Zhang, "Formulation of error propagation and estimation in grating reconstruction by a dual-rotating compensator Mueller matrix polarimeter," Thin Solid Films (published online 2014).
[25]M. Foldyna, A. De Martino, E. Garcia-Caurel, R. Ossikovski, F. Bertin, J. Hazart, K. Postava, and B. Drévillon, Phys. Status Solidi A **205**, 806 (2008).